buildings

MDPI

Article

Damaged Masonry Structures: A Probabilistic Approach for Fast Structural Safety Assessment †

Elsa Garavaglia , Giuliana Cardani and Danila Aita *

Department of Civil and Environmental Engineering, Politecnico di Milano, 20133 Milan, Italy; elsa.garavaglia@polimi.it (E.G.); giuliana.cardani@polimi.it (G.C.)
* Correspondence: danila.aita@polimi.it; Tel.: +39-02-23996615

† This paper is an extended version of our paper published in Garavaglia, E.; Cardani, G.; Aita, D. On the Safety of Damaged Masonry Structures: A First Probabilistic Approach. In Proceedings of the 4th International Conference of Steel and Composite for Engineering Structures. ICSCES 2025, Piacenza, Italy, 9–12 July 2025; Lecture Notes in Civil Engineering; Milani, G., Magagnini, E., Khatir, S., Eds.; Springer: Cham, Switzerland, 2025; Volume 746, pp. 725–733.

Abstract

Structural safety assessment of masonry structures is a crucial topic for architectural heritage conservation. Performance indicators are commonly adopted for civil structures and infrastructure made of reinforced/prestressed concrete or steel but are often overlooked in the context of historic structures. Notions such as safety, reliability, robustness, and resilience are accepted concepts in the world of historic buildings, but they rarely translate into quantifiable indicators applicable to structural rehabilitation. The complex mechanical behaviour of masonry, indeed, is affected by uncertainties in the characterization of the material's properties. Furthermore, when considering damaged masonry structures, uncertainties also include the natural aging and degradation of the component materials. In this context, the proposed research intends to perform a preliminary safety assessment of a masonry building subjected to seismic loads considering a given damage level and its evolution over time. Damage is described by means of a performance parameter that is able to capture the decrease in the characteristic compressive strength related to the presence of a crack pattern and changes in the live loads. The method allows one to address in a probabilistic way the determination of a limit global safety factor, affected by this parameter, and of the time required to attain the failure condition.

Keywords: masonry; seismic behaviour; damage; time of failure; global safety factor; static safety factor; fragility curves; reliability; probabilistic approach

Academic Editor: Duc-Kien Thai

Received: 23 December 2025
Revised: 11 February 2026
Accepted: 22 February 2026
Published: 27 February 2026

1. Introduction

As is well known, seismic events are extremely damaging to structures, with significant social and economic consequences. Large-scale seismic vulnerability assessment is crucial for mitigating potential damage from future earthquakes. The interest on this topic is testified by a number of research, starting with [1–3], who propose an operational methodological protocol for the seismic classification of existing masonry buildings for practitioners, along with the studies proposed by [4], where various seismic damage scenarios at a territorial scale were presented in order to examine distinct housing typologies and an updated version of the vulnerability index method was used to create the seismic vulnerability assessment. More recently, Reference [5] suggests an integrated strategy that combines census data, GIS software, and satellite remote sensing; risk assessment was carried out using Multi-Criteria Decision-Making techniques. For an in-depth review of the most important research on this topic—outside the scope of the present contribution—the interested reader is directed to [6], where seismic risk assessment at a national scale is traced back to the combination of three components: seismic hazard, structural vulnerability, and exposure data. A common denominator of these studies is the relationship between the vulnerability class and the expected damage level and seismic intensity; see also [7,8]. The interest in developing tools to support seismic retrofit strategies of existing buildings is demonstrated by recent contributions; see for example [9], who are focused on a resilience-based approach. Other important aspects related to the assessment of seismic vulnerability in general are the construction of analytical fragility curves developed based on the probability of exceeding the failure limits for each scenario [10–12], and the consideration of epistemic uncertainties [13].

In this context, the current research introduces an innovative approach for the initial safety assessment of a masonry building subjected to seismic forces. The aim is to contribute to a rapid and non-invasive "survey" of the structural safety of masonry structures, which is essential for developing strategies for the conservation of historic minor architectural heritage. This method considers a specific degree of damage through a performance parameter capable of characterizing both the decrease in the characteristic strength values (related to the presence of a crack pattern caused by variable loads) and how it changes over time. Finding an appropriate law for the performance parameter is essential to adequately capture the cracking evolution. As will be described in this article, it is necessary to define a damage onset time and a subsequent damage evolution law that is intrinsically non-deterministic. The procedure aims to define a global safety factor influenced by the damage parameter and, in a probabilistic framework, to estimate the time required to reach the "limit" condition. This method allows for a reliable assessment of the overall vulnerability of a city's residential historical building stock, starting from the methodology of data survey based on CARTIS form, observed building by building. As an example, Figure 1a shows an extensive vulnerability assessment campaign for the ordinary residential buildings in masonry that characterize a large part of the historic centres of Milan hinterland (Figures 1b and 2). The results of this approach should form the basis for targeted and in-depth investigation on this architectural heritage [14].

(**a**) (**b**)

Figure 1. Milan hinterland (Paullo, Italy): (**a**) fast and non-invasive investigation method for the acquisition of a picture of the overall level of vulnerability of the residential built heritage of a city; elaborated from [15]; (**b**) example of masonry buildings with the insertion of large openings on the ground floor.

(a) (b) (c)

Figure 2. Example of recurrent residential masonry houses in the historic centres of Milan hinterland (in Paullo): (**a**) one with a brick masonry vault at ground floor; (**b**) simple buildings arranged around an open courtyard and (**c**) in a row along the street.

The starting point for the development of the method is the contribution provided in [16] where, using a model found in the literature [1–3] and devising a probabilistic method to evaluate the global safety factor and the static safety factor when the seismic, topographic, and subsoil conditions of the site vary, the authors underlined the importance of some performance parameters found in the calculation process suggested in [1,3], whose randomness can influence the estimation of these factors.

For a fast method of characterizing load-bearing masonry, it is considered appropriate to refer to the values specified by the technical standards for constructions. For the main types of masonry present in the Italian national territory, the CNR-DT 212/2013 regulation [17] suggests reference values to be used as stochastic characterization of their mechanical properties. These values are derived from those suggested in Table C8A.2.1 of [18] and Table C8.5.1 in [19], which are sources of statistical information.

The data contained in the above-mentioned standards show that the characteristic strength parameters present a certain degree of uncertainty for each type of masonry, due to their non-standard constructive techniques. The impact of these parameters on the evaluation of the global and static safety factors is examined in [15], where the analysis of the shear and compressive strength characteristics was introduced with reference to the indications reported in CNR-DT 212/2013 [17] and their impact on the variation in the safety factors was investigated through the creation of a fragility curve.

A crucial factor in assessing the safety and reliability of a structure is the ability to estimate its future lifespan based on the degree of damage already suffered. The definition of an instant of damage triggering and a subsequent temporal evolution that is intrinsically non-deterministic are necessary to describe the evolution of the crack pattern.

The study here proposed, extending the contribution presented in [20], intends to investigate these aspects. It is organized as follows. In Section 2.1, the concepts of global safety factor and static safety factor are recalled, introducing the approach further developed by the current research. In Section 2.2, attention is paid to the performance parameter "f" of the reduction in characteristic strength values as a function of the presence or absence of a crack pattern. Section 2.3 illustrates the novel probabilistic method aimed at capturing the specific level of damage reached by the building by assuming "f" as a parameter varying over time according to an evolutionary law derived from the evidence of experimental tests of long-term behaviour conducted in a laboratory on existing masonry samples [21–23]. Sections 3–6 depict the results of such an approach by considering a case study and proposing some further methodological developments. More specifically, Section 3 presents the estimation of the global and static safety factors as a function of parameter "f" and time. Furthermore, it examines the estimation of the probability of failure and the resulting loss of reliability and safety. Section 4 focuses on estimating the waiting time for two different threshold transitions, considering how the triggering of further damage compromises the safety factor and the resulting failure time. Section 5 studies the effects of a structural aggravation action on a building system subjected to an existing crack pattern; this analysis is further developed in Section 6, where the safety factor and failure time in the case of subsequent damage triggers are investigated. Near the end, Section 7 provides a discussion on the uncertainties affecting the problem. Concluding remarks and further development of the research are described in Section 8.

2. A Time-Varying Law Describing Loss of Performance

In Section 2.1, the methodology proposed by Borri et al. in [1–3] is briefly presented in order to fully clarify the starting point of the new development proposed by the current contribution and to adopt a univocal notation. Section 2.2 illustrates the role of the performance parameter "f" in the structural response of damaged masonry structures. In Section 2.3, a new probabilistic approach is illustrated with regard to the methodological aspects and the definition of a law describing the performance loss of the system over time.

2.1. Global Safety Factor and Static Safety Factor: A Brief Review

The treatment devised by Borri et al. [1,3] is based on the concepts of global safety factor, SF_G, and static safety factor, SF_S. The first one is the ratio between the ultimate acceleration related to each floor i of the building, $a_{SLU,i}$, and the maximum ground acceleration, a_g, referring to the seismic zone and the return period considered according to the equation

$$SF_{G,i} = \frac{a_{SLU,i}}{a_g \cdot S}, \tag{1}$$

where S is the spectral coefficient that characterizes the area from the subsoil and topographic point of view.

Compared to the formulation contained in [18,19,24,25] (more precise from a theoretical point of view but more costly to apply, especially when there are many buildings to examine), References [1,3] propose some simplifications in favour of safety.

It is recalled that $a_{SLU,i}$ depends on the shear strength at the base of each floor i, $F_{SLU,i}$, according to the following relation:

$$a_{SLU,i} = \frac{r\,q\,F_{SLU,i}}{e^*\,M\,F_0}, \tag{2}$$

where

- r is a correction factor that accounts for the numerous simplifications adopted, in favour of safety. It is equal to 1.0 for buildings with one story above ground and equal to 2.0 for buildings with two or more stories above ground.
- q is the behaviour factor; it takes into account the dissipative features of the building (Appendix A.1).
- e^* is the mass participation factor, which depends on the vibration modes and the participating mass (Appendix A.2).
- M is the total seismic mass of the building.
- F_0 is the spectral amplification factor.

$F_{SLU,i}$ is calculated as the smallest of those evaluated in two perpendicular directions, generally chosen on the basis of the main axes, indicated by x and y, of the load-bearing walls. For each direction, the vertical load-bearing masonry panels are considered; collapse is reached when the mean shear stress reaches an appropriate proportion of the shear strength of the masonry material. Therefore, the formal expression of the building shear capacity can be written according to relations (3) and (4), depending on the axis considered:

$$F_{SLU,ix} = \frac{0.8\ \xi_x A_{xi} \tau_{di}}{1.25}, \tag{3}$$

$$F_{SLU,iy} = \frac{0.8\ \xi_y A_{yi} \tau_{di}}{1.25}, \tag{4}$$

where

- A_{xi} (resp. A_{yi}) is the shear-resistant area of the walls of the i-th floor, arranged in the x (resp. y) direction.
- ξ_x (resp. ξ_y) is a coefficient linked to the type of failure expected in the masonry walls of the i-th floor; it is equal to 1 in the case of shear collapse, while it can be assumed to be equal to 0.8 in the case of collapse due to combined compressive and bending action (buckling).
- τ_{di} is the design value of the shear strength in the masonry walls of floor i. It depends on the value of the masonry shear strength, $\tau_{0,d}$, and on the average vertical compressive stress, $\sigma_{0,i}$, recorded on the horizontal section of the walls at the i-th floor.

Note that in Equations (3) and (4), some coefficients related to the irregularity of the plane and to the homogeneity of stiffness and resistance of the masonry walls are set to their worst possible values, i.e., 1.25 and 0.8 respectively, in favour of safety. This simplification is necessary to allow a rapid application of the method for seismic classification and when direct data of the buildings are unknown.

To evaluate the mass M, both the weight of the masonry walls and the load related to each floor must be considered. The latter includes the self-weight of the floor, the permanent loads, and the live loads.

The global safety factor to be considered for the vulnerability assessment of the building is the lowest value among the $SF_{G,i}$ values determined for each floor i; see Equation (1):

$$SF_G = SF_{G,\min} = \min SF_{G,i} \tag{5}$$

The static safety factor at each floor, $SF_{S,i}$, can be defined as a percentage of the compressive stress limit, σ_{RD}, according to the relation:

$$SF_{S,i} = \frac{\sigma_{RD}}{\sigma_{0,i}}, \tag{6}$$

where $\sigma_{0,i}$ is the average compressive stress recorded at each floor, as defined with reference to Equations (3) and (4). The expression of σ_{RD} is given by:

$$\sigma_{RD} = \frac{0.65\ f_m}{\gamma_M\ CF}, \tag{7}$$

where f_m is the average compressive strength of the masonry, γ_M is the safety factor on the material, and CF is the confidence factor dependent on the level of knowledge achieved.

The minimum value among the $SF_{S,i}$ values obtained for each floor i (see Equation (6)) must be taken into account for safety reasons:

$$SF_S = SF_{S,\min} = \min SF_{S,i}. \tag{8}$$

2.2. Undamaged Masonry Versus Damaged Masonry: The Role of the Parameter f

The method introduced so far can describe the safety level of an undamaged masonry structure. When evaluating the SF_G and SF_S safety factors, it is also possible to consider the case of damaged masonry by introducing a damage parameter that quantifies the reduction in the masonry's structural capacity to both horizontal and vertical forces.

Therefore, the method proposed by [1–3] can be further implemented by introducing a strength reduction factor, f, in the case of damaged masonry. The factor will be introduced in the expressions of both the design value of the shear strength,τ_{di}, and of the compressive stress limit, σ_{RD}.

To show how the f parameter can influence the evaluation of τ_{di} and σ_{RD}, reference is made below to the formulations proposed by Borri et al. [3] and the Italian technical standard [17] (see Appendix A.3). Note, however, that the procedure described is general and can be applied considering standards other than the Italian one. Despite the multiple interpretations that can be given to the concept of damage, for the purposes of this work, it is emphasized that it can determine first of all a reduction in the strength of the material, as described by [26], who investigate the influence of moisture content and salt concentration on the strength of bricks, and by [27], who underline how geometric degradation (such as the reduction in the filling of mortar joints) influences both the failure mechanism and the stiffness and strength of the masonry material.

Introducing a damage parameter, f, the expressions of τ_{di} and σ_{RD} become

$$\tau_{di} = \frac{\tau_{0,d}}{CF} \cdot f \sqrt{1 + \frac{\sigma_{0,i}}{1.5 \frac{\tau_{0,d}}{CF} \cdot f}}, \tag{9}$$

$$\sigma_{RD} = \frac{0.65\, f_m}{\gamma_{\mathrm{M}}\, CF} \cdot f \tag{10}$$

The strength reduction factor, f, can be defined as a performance parameter able to reflect the masonry integrity $(f = 1)$ or damage $(0 < f < 1)$, which affects the building seismic behaviour. In the treatment proposed by Borri et al. [1,3], the performance parameter, f, is taken to be 0.8 for damaged masonry and 1 for undamaged masonry. The assumption of two distinct values for the parameter f leads to a deterministic evaluation of the building safety.

In the following section, a probabilistic approach is proposed that is capable of taking into account the randomness of the quantities involved. This approach, although streamlined and not entirely exhaustive, can offer a tool for the rapid assessment of a building vulnerability, through the construction of fragility curves.

2.3. A Novel Probabilistic Approach: The Performance Parameter f as a Time-Varying Parameter

Studying a building history from the time of its construction to the present, tracking its changes over the ages, and particularly looking into the most recent interventions can reveal periods when the stresses on the masonry walls may have changed significantly, which over time, may cause weakening of the structure and the development of cracks. There are many causes that can lead to the onset of an evolving crack pattern, for example, replacing original wooden floors with modern ones with increased weight, changing the intended use of the building, inserting large openings on the ground floor with fewer masonry walls bearing capacity, etc.; see Figure 1b. Due to one or all of these causes, it can be assumed that the performance parameter f varies over time, showing an evolving crack pattern. It is not an easy matter to define an evolutionary law capable of describing the evolution of the damage. Indeed, there are a lot of uncertainties:

- The triggering time at which cracking begins (historical records can help identify one or more moments of damage initiation, such as a seismic event or some renovation work that weakens load-bearing structures).

- Damage evolution law (even if accelerated, laboratory and on-site tests can offer helpful indications on the evolution of a particular damage process).
- Failure time.

When the crack pattern begins, the performance parameter, f, must be able to detect the change in the performance of the system and decrease proportionally following an appropriate damage evolution law.

A possible evolution of the performance parameter f over time can be described by the following relationship:

$$f = f(t) = f_0[1 - \delta(t)], \tag{11}$$

where f_0 is the value of the performance parameter at time $t = 0$ (e.g., initial state), and $f(t)$ indicates the value of f as time and damage evolve. More precisely, the quantity $1 - \delta(t)$ measures how f decreases over time in accordance with a predetermined time variant damage law, $\delta = \delta(t) \in [0, 1]$. It is important to define the latter in a way that is sufficiently reliable, taking into account that it must be sufficiently flexible to adjust to the randomness of the evolutionary behaviour.

Among other possibilities, the law put forth by [28–30] might address the fundamental requirements described above:

$$\delta(\tau) = \begin{cases} \omega^{1-\rho}\ \tau^{\rho} & ,\ \tau\ \leq\ \omega \\ 1 - (1-\omega)^{1-\rho}\ (1-\tau)^{\rho} & ,\ \omega\ <\ \tau\ <\ 1 \\ 1 & ,\ \tau\ \geq\ 1 \end{cases} \tag{12}$$

In Equation (12), ρ and ω are damage parameters that define the damage evolution law shape; they must be chosen according to the actual evolution of the damage process; $\tau = \frac{t}{T_f}$ is the normalized evolution time, where T_f is the failure time, i.e., the time instant of reaching the failure threshold, $\delta = 1$.

Regarding the definition of the failure time, T_f, it is important to note that it varies depending on the phenomenon under consideration. In the literature, it is occasionally assumed that the failure time has a Weibull or Gamma probability distribution law [16]. The choice, however, is not simple; the distribution law of T_f, hereinafter referred to as F_{Tf}, must be able to describe the physical behaviour of the phenomenon being studied, even for rare, difficult-to-predict events that are normally found in the tails of the distributions themselves. These events are captured by studying the immediate occurrence rate function, $\lambda_j(t)$, of the distributions, a function that can predict the probability that the studied event will occur in the interval (t + dt) immediately following the current time, t, if it has never occurred at times prior to t.

$$\lambda_j(t)dt = Pr\{t < \tau_j \leq t + dt | \tau_j > t\}, \tag{13}$$

where τ_j is the time at which the transition of the j-th data level could occur.

Reaching and exceeding a certain level of damage, in the absence of catastrophic situations, is a progressive physical phenomenon, and the probability that a certain damage threshold will be exceeded immediately increases with the waiting time. Probability distributions that exhibit an immediate occurrence rate that increases over time include the Weibull and Gamma distributions, so researchers have been focusing on these two distributions for some time [31,32].

Moreover, to define a reliable damage law, the parameters must be determined on the basis of plausible evolutionary behaviour.

In this research, reference is made to the experimental analyses proposed by [21,22], where the values of the strain rate variation caused by the permanence of long-term static loads on samples of historical masonry are reported (Figure 3). From these tests, stress–strain and strain–time diagrams are derived for both the vertical and horizontal directions. For the purpose of the present study, a significant result of the experimental investigation described by [21,22] is to demonstrate a link between the evolution of the strain rate and that of the crack pattern. This finding is further supported by some recent studies [33,34], where the relationship between the global stiffness of the structure and the evolution of cracking is examined. Figure 3a shows both vertical and horizontal strain over time under different steps of vertical loads: changes in the strain rate indicate a worsening of the crack pattern until collapse (Figure 3b). Figure 4, obtained by reworking the results reported in [21,22], shows the variation in the vertical strain with time for long-term constant static load (the results related to different historic masonry specimens are plotted in different colours).

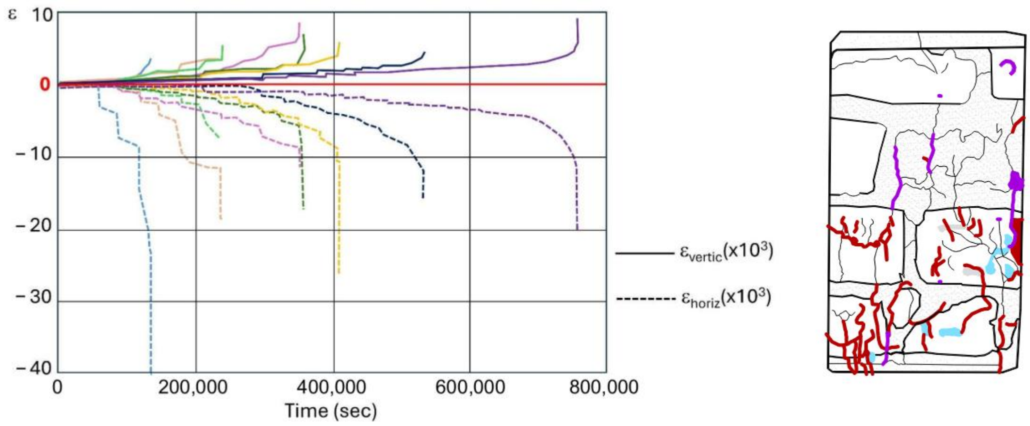

(**a**) (**b**)

Figure 3. Pseudo-creep tests on samples of historical masonry: (**a**) pseudo-creep curves (the results related to different specimens are plotted in different colours) and (**b**) example of crack pattern at the end of tests. Elaborated by the authors from [21].

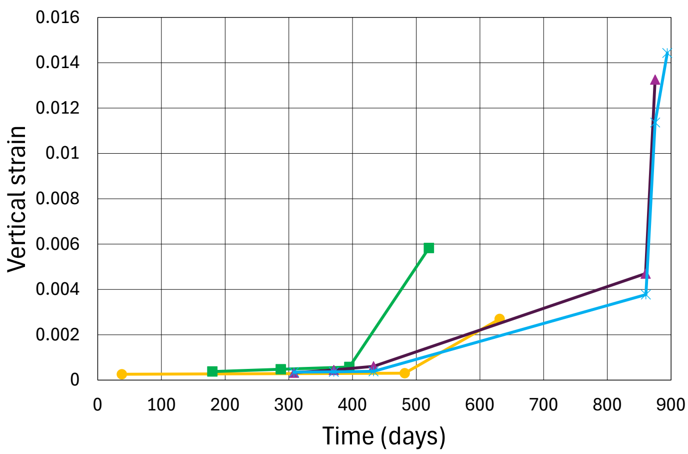

Figure 4. Long-term constant static load: variation in the vertical strain with time. The results related to different historic masonry specimens are plotted in different colours (data elaborated by the authors from laboratory tests in [21,22]).

Given the above, the damage law $\delta(\tau)$ can be hypothesized by considering the laboratory results. Figure 5a plots a theoretical damage curve $\delta(\tau)$ (see the black solid line) that satisfies a similar trend to that of Figure 4, as shown by a comparison with the normalized laboratory values (see the coloured dots). As regards the mathematical definition of

$\delta(\tau)$, it is assumed that the damage parameters of the damage evolution law shape (see Equation (12)), ρ and ω, have a normal probability distribution law, F_ρ and F_ω, respectively. The values of ρ and ω, assumed to be the mean of the normal distribution, $\rho = 5.5$ and $\omega = 0.93$, were obtained from experimental data through least squares optimization; the estimation error was used as a parameter measuring the standard deviation. Their quantification can be refined if homogeneous and reliable databases are available. The use of Bayesian approaches to improve knowledge can also certainly make the degradation law more robust.

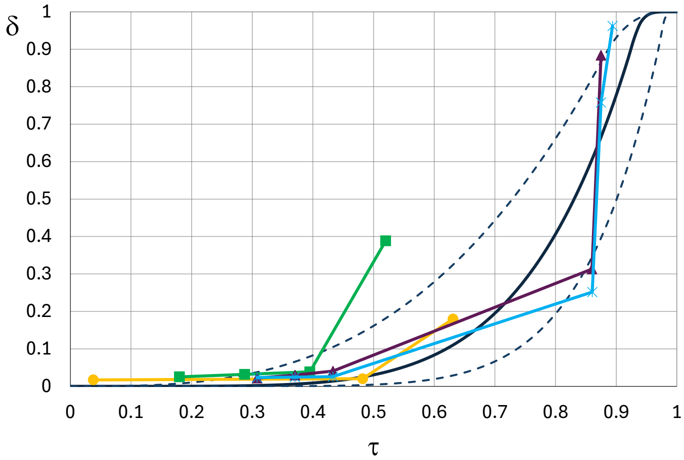

(**a**)

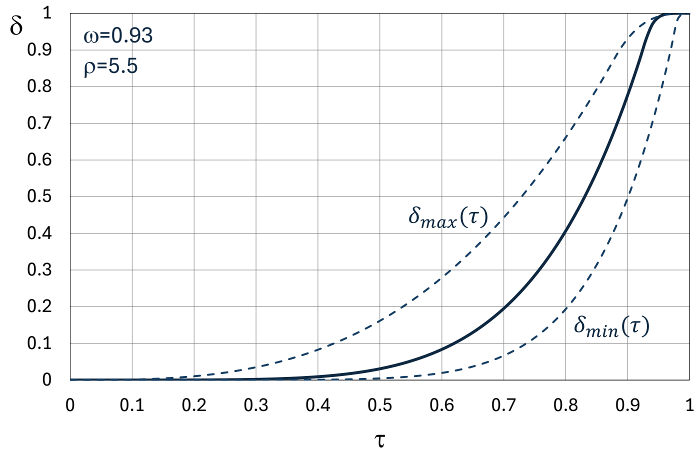

(**b**)

Figure 5. Proposal of a damage law (δ) following the trend of laboratory results (Figure 4): (**a**) normalized laboratory values and theoretical law; (**b**) the same damage law considering the mean ω and ρ values (solid line) and the limits of the range (dashed lines), $\delta_{\min}(\tau) \le \delta(\tau) \le \delta_{\max}(\tau)$.

The black solid curve in Figure 5b is obtained by taking into account the mean values of the shape parameters ($\rho = 5.5$ and $\omega = 0.93$), while the limit curves—defined by the mean values of the shape parameters plus and minus their standard deviations—are shown by the dashed curves. Note that the uncertainty that characterizes the estimate of the parameters ρ and ω corresponds to the range $\delta_{\min}(\tau) \le \delta(\tau) \le \delta_{\max}(\tau)$ within which the complete set of damage laws used to explain the phenomenon is included.

Figure 6 shows the flowchart of the procedure described above for determining the static safety factor, SF_S, and the global safety factor, SF_G, considering a given damage law as the one proposed in Equation (12), which influences the evolution of the performance parameter f; see Equation (11). Figure 7 depicts a flowchart of the inputs necessary to define the damage law $\delta(\tau)$, i.e., the probability distributions F_ρ and F_ω, for the damage parameters ρ and ω (normal probability distribution law) and F_{Tf} for the failure time T_f

(Weibull or Gamma distributions). For any j-th damage law belonging to the set described above, in the interval $\delta_{\min}(\tau) \leq \delta(\tau) \leq \delta_{\max}(\tau)$, the corresponding performance parameter, $f = f^j$, is obtained from Equation (11). It is therefore possible to calculate the static and global safety factors for any f^j.

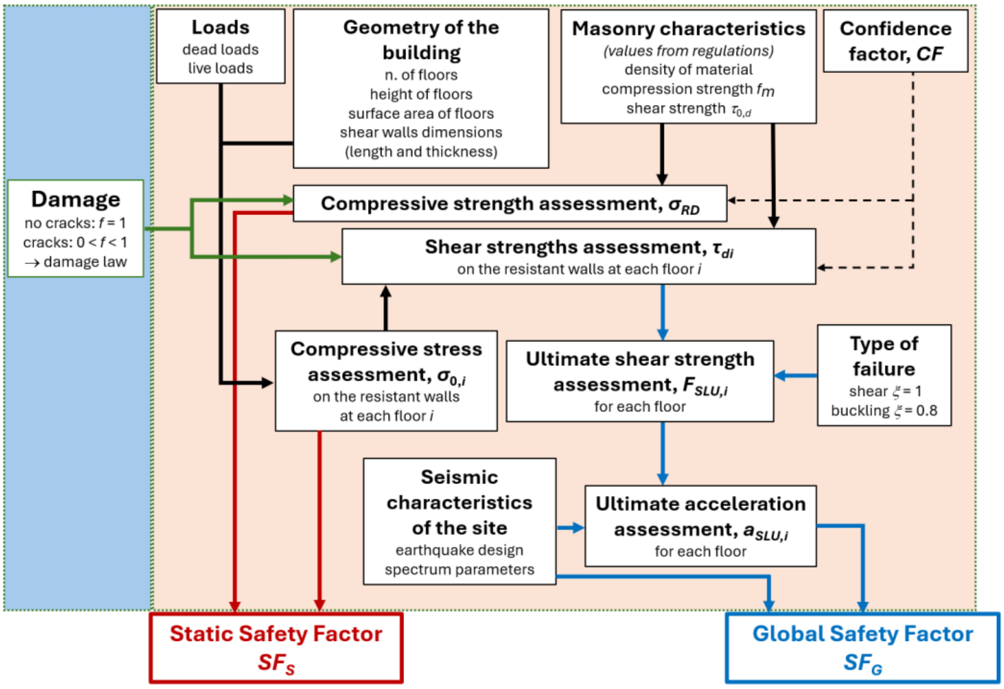

Figure 6. Flowchart of the procedure for determining the static safety factor, SF_S, and of the global safety factor, SF_G, considering a damage law.

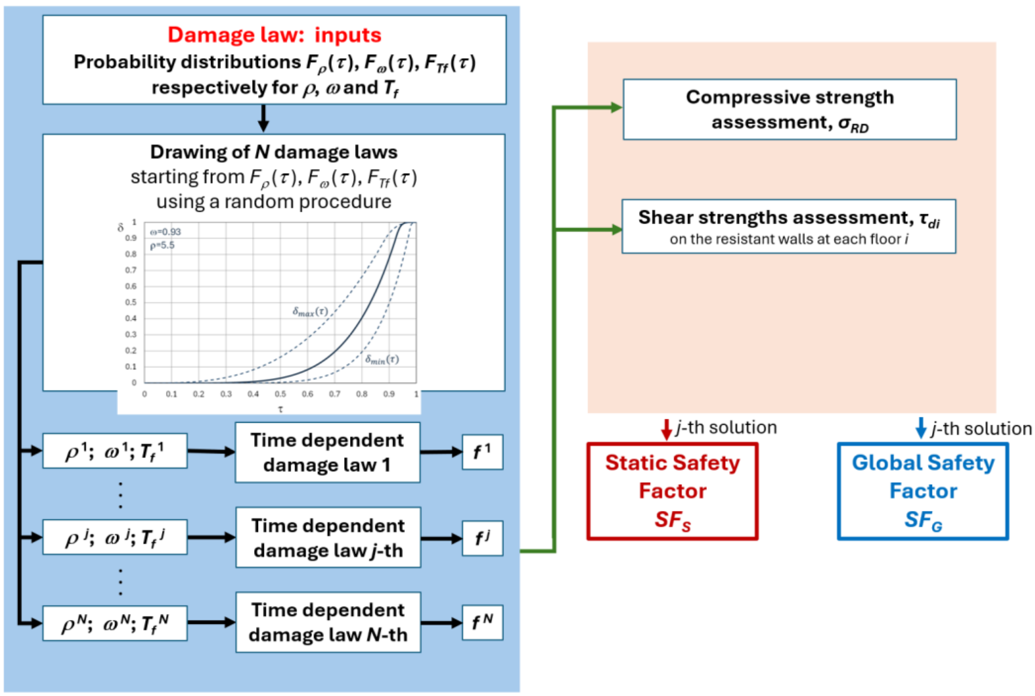

Figure 7. Flowchart of the inputs needed to define the damage law $\delta(\tau)$: F_ρ, F_ω, and F_{Tf}. For each j-th damage law, the corresponding performance parameter, f^j, and the static and global safety factors are retrieved.

3. Variation in the Global Safety Factor and the Static Safety Factor over Time and Assessment of the Reliability of the Building System

As previously stated, variations in the static configuration are the primary cause of the uncertainties in the estimation of the parameter f and, consequently, of the global and static safety factors, SF_G and SF_S. These uncertainties are primarily associated with the instant of damage triggering. In this section, an initial evaluation of the trend of the safety factors SF_G and SF_S, with random variations in the parameter f after the damage onset time, is examined with reference to a case study, i.e., typical historical masonry buildings in the Lombardy lowland area (Figure 2). For the purposes of this investigation, it is assumed that the buildings are located in the Lombardy region, in the eastern area, where there is the seismic zone 2 according to Italy's anti-seismic regulations [18,19,24,25,35], with peak ground acceleration in the range 0.15 $g < a_g \leq 0.25$ g, where a_g corresponds to the acceleration with a 10% probability of being exceeded in 50 years. As regards the seismic characteristics, reference is made to those of the municipality of Salò (BS), Lombardy's most seismically active area; see Table 1 [20] and Appendix A.4. It is interesting to recall that for this specific building typology, the analyses had highlighted a certain fragility even when adopting the parameter f = 1 (undamaged masonry) [16].

Table 1. Seismic characteristics of the Salò town (BS), eastern Lombardy (Italy).

Seismic Characteristic	Symbol
Peak acceleration (maximum expected horizontal acceleration at the site)	$a_g = 0.158$ g
Spectral value (characteristic of the constant velocity section)	$T_C^* = 0.271$ s
Seismic return period	$T_R = 475$ years
Maximum value of the spectrum amplification factor in horizontal acceleration	$F_0 = 2.483$

Assuming the damage initiation at an instant T_1 of the structure lifetime, from a plausible Gamma distribution curve of the structure lifetime, eleven instants, t, after the instant T_1 have been extracted and subsequently normalized $\left(\tau = \frac{t}{T_f}\right)$; see Figure 8 (the normalized form of T_1 is assumed to coincide with $\tau = 0.4$; see Figure 8b).

For each normalized instant τ, the value of the decrease for the performance factor, $f(\tau)$, due to the crack initiation, is obtained from Equation (11).

The proposal to associate the time of onset of the first damage, T_1, with the value $\tau = 0.4$ stems from experimental data derived from the laboratory tests that served as the foundation for the construction of the damage curve. It should be noted that the damage triggering time could also be related to the value $\tau = 0$ or to other values of τ, if more precise information were available on the history of the building under examination.

The probabilistic approach developed within this research is capable of capturing the randomness of the value of $\delta(\tau)$ at any instant τ (Figure 8). A random extraction of 100 values of δ between $\delta_{\min}(\tau)$ and $\delta_{\max}(\tau)$ is made for each of the eleven normalized instants τ. The value of $f(\tau)$ for each extracted τ and each value of δ is then retrieved from Equations (11) and (12).

The safety factors SF_G and SF_S associated with τ and $f(\tau)$ are then determined using the methodology suggested by [1,3], as described in Section 2 (see Equations (5) and (8), taking into account Equations (9) and (10)). Such safety factors are implemented with a progressive calculation macro used by Borri et al. [1,3] for the assessment of the seismic vulnerability of historical centres.

The trend of both safety factors, SF_G and SF_S, reported in Figure 8, corresponds to a progressive loss of performance over time. In Figure 8a, related to SF_G, the solid black line represents the mean value; the dashed lines delimit the range identified by the mean + and − the standard deviation. The solid black horizontal lines in both plots indicate the limit thresholds of possible failures, $SF_{G,failure}$ and $SF_{S,failure}$ respectively. Both safety factors are expressed as a percentage. As regards the global safety factor, SF_G, the limit that identifies failure is set at 20%; see also [3,16]; for the static safety factor, SF_S, it is 200%. It is worth noting that the static safety factor values exceed 100% in almost all cases under examination (see Figure 8b), and this represents a large "static" safety margin related to the compressive strength of masonry. When calculating SF_S, values significantly higher than 100% (the minimum expected safety level for static behaviour) are often reached because masonry structures were traditionally oversized for safety reasons. Note that in Figure 8a,b, the stochastic values of the safety factors are provided for each of the eleven normalized instants τ, as described at the beginning of this section.

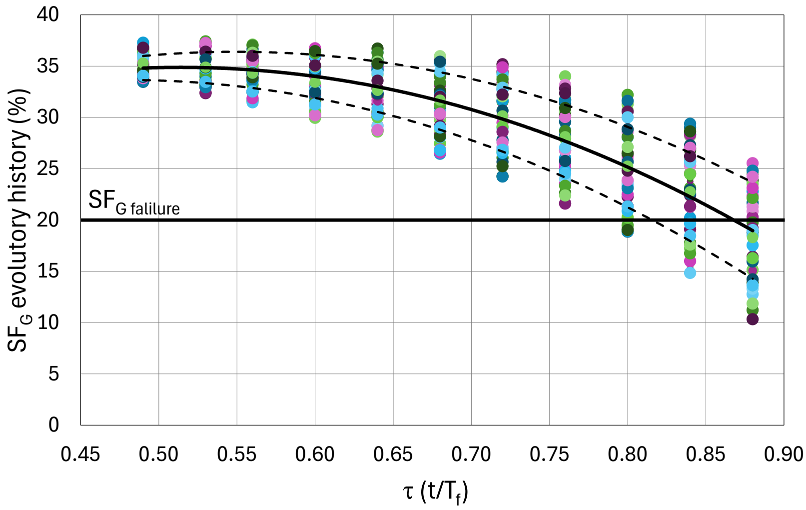

(**a**)

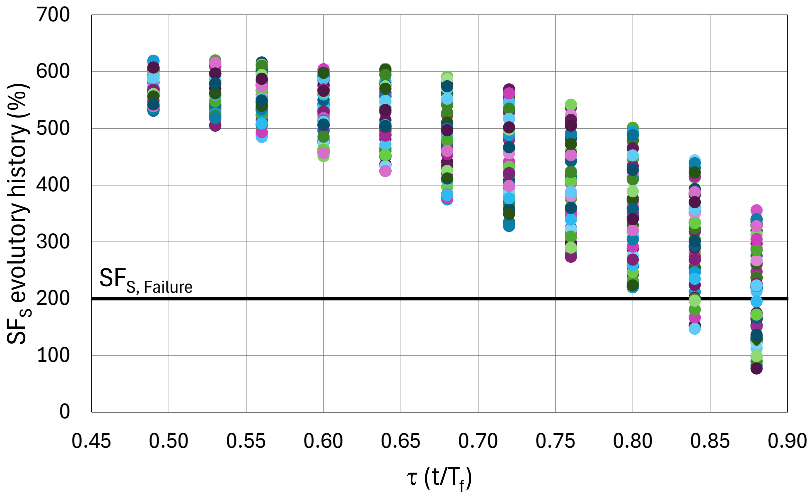

(**b**)

Figure 8. Trends of the safety factors SF_G (**a**) and SF_S (**b**) considering the reduction in the performance parameter $f(\tau)$ over time. The limit thresholds related to possible failures, $SF_{G,failure}$ and $SF_{S,failure}$, are indicated by the solid black horizontal lines.

For the purpose of this research, the method is illustrated below considering the trend of the SF_G factor as a performance indicator of a possible failure, as it seems reasonable for the typology under consideration; see also [16]. The procedure can be easily applied with reference to SF_S.

The next stage of the proposed methodology consists of estimating the probability of failure and the consequent decrease in safety and reliability.

Before proceeding further, it is necessary to clearly define the concept of reliability of a system. Following the definition given in [36], reliability can be explained as the probability that the system will not collapse at time t.

This definition is adapted to the context under consideration, denoting by $R(\tau)$ the reliability of the building, i.e., the probability that the SF_G value is higher than a pre-set "failure" limit considering a selected threshold of significant damage occurring at the normalized instant τ. Let τ be chosen as the random variable. The reliability is expressed by the following relation:

$$R(\tau) = Pr\left\{SF_G(\tau) > SF_{G,failure}\right\} = 1 - F_{SF_G}(\tau), \tag{14}$$

where $F_{SF_G}(\tau)$ is the cumulative distribution of SF_G. To perform the reliability assessment of the system, the values of the global safety factor SF_G recorded at each normalized instant τ are modelled according to a probabilistic approach. In the present study, a Lognormal distribution is assumed. With reference to Figure 9, the probability density functions that model SF_G for each τ and the horizontal line corresponding to the pre-set failure threshold, $SF^* = SF_{G,failure}$, are shown. The areas enclosed by such densities and above the horizontal line (see Figure 9a) represent the experimental probabilities that are part of the construction of Equation (14); see Figure 9b.

Figure 9b shows the experimental reliability function, obtained by means of Equation (14), for each value of the extracted normalized instants τ. Each point quantifies the value of the areas defined above for each extracted τ (Figure 9a). The experimental reliability function thus obtained is then modelled by considering a theoretical probability Gamma distribution (solid line in Figure 9b).

Choosing distributions to model specific physical phenomena is always a delicate and complex process. The distributions we propose in this paper are the result of previous studies in the literature [37–41], which have convinced us of their suitability, but they are not intended to be definitive. Future research and experimental tests may guide us toward other solutions.

The results here obtained show that the initiation of damage can lead to a long-term loss of performance even without further increases in loads, as observed in laboratory tests in [21]. In this instance, assuming that the damage was caused at the instant $\tau^* = 0.4$ (i.e., 40% of the structure's lifetime), such that $t^* = 0.4\ T_f$, it is reasonable to assume that the chance of achieving a global safety factor near the threshold $SF^* = 20\%$ (see Equation (1)) can happen in an interval of time that is nearly equal to the trigger time $\tau = 0.865$. Indeed, as can be seen from Figure 9a, near the normalized instant $\tau = \tau_{risk} = 0.865$, the risk of reaching a global safety factor close to the threshold of 20% of the overall performance of the structure occurs, and as a consequence, the 20% threshold could be reached in the interval $0.82 < t_{20\%} < 0.90\ T_f$ (approximately the upper and lower limits of the range defined by the dashed curves in Figure 9a). However, the building will undoubtedly experience additional changes during its remaining life, and both the reliability function performance and the failure prediction may change.

The reliability coefficient β can be calculated as proposed by [40]:

$$\beta(t) = \frac{\mu_R(t) - \mu_D(t)}{\sqrt{\sigma_R^2(t) + \sigma_D^2(t)}}, \tag{15}$$

where the numerator is the average of the system response to the imposed stresses, $\mu_R(t)$, minus the average of the performance demand required from the system, $\mu_D(t)$, while the denominator shows the square root of the sum of the squares of the respective standard deviations, $\sigma_R^2(t) + \sigma_D^2(t)$, all calculated at each instant t of the structure lifetime, T_f.

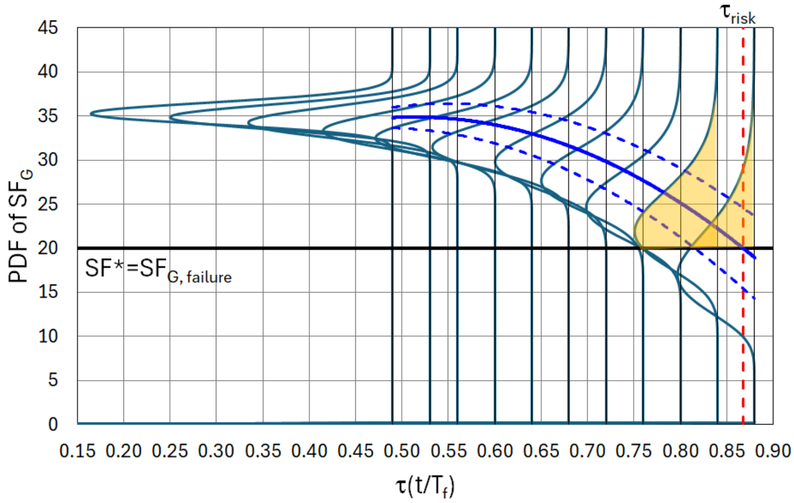

(**a**)

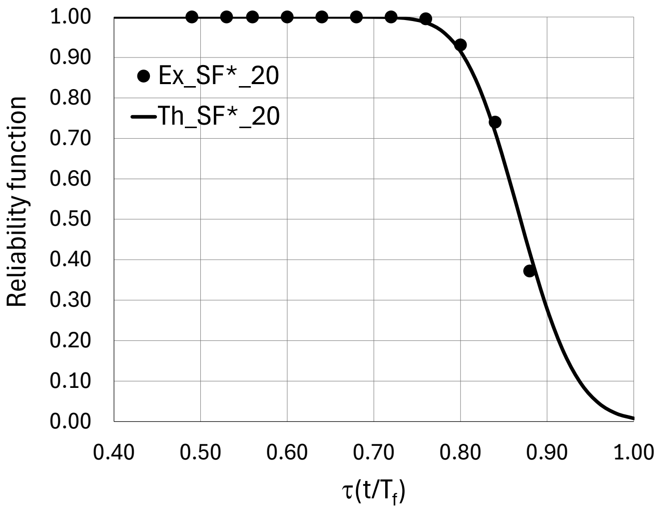

(**b**)

Figure 9. (**a**) Probabilistic modelling of the SF_G value distributions at each instant τ and as a result of the performance parameter f's random variation. (**b**) The experimental reliability function (dotted) is modelled with a theoretical probability distribution of the Gamma type (solid line). $SF^* = 20\%$ is the fixed threshold for the global safety factor. The points of the experimental curve in (**b**) correspond to the areas enclosed by the PDF and above the horizontal line in (**a**) (for example, the areas coloured in orange).

In the case studied, assuming a fixed threshold as performance demand, given by $SF_G = SF^* = SF_{G,failure} = 20\%$ (see Figure 9a), (15) is modified into:

$$\beta(\tau) = \frac{\mu_{SF_G}(\tau) - SF_{G,failure}(\tau)}{\sqrt{[\sigma_{SF_G}(\tau)]^2}}. \quad (16)$$

Note that in (16), reference is made to the normalized time, $\tau = \frac{t}{T_f}$.

Figure 10 shows the experimental trend of the values of $\beta(\tau)$ evaluated at the eleven extracted values of τ, already considered in the probability density plots of Figure 9a. The experimental results were fitted with a polynomial function that optimizes the parameters using the least squares method:

$$\beta(\tau) = -a\tau^2 + b\tau + c \tag{17}$$

with $a = 43.74$; $b = 9.77$; and $c = 17.55$.

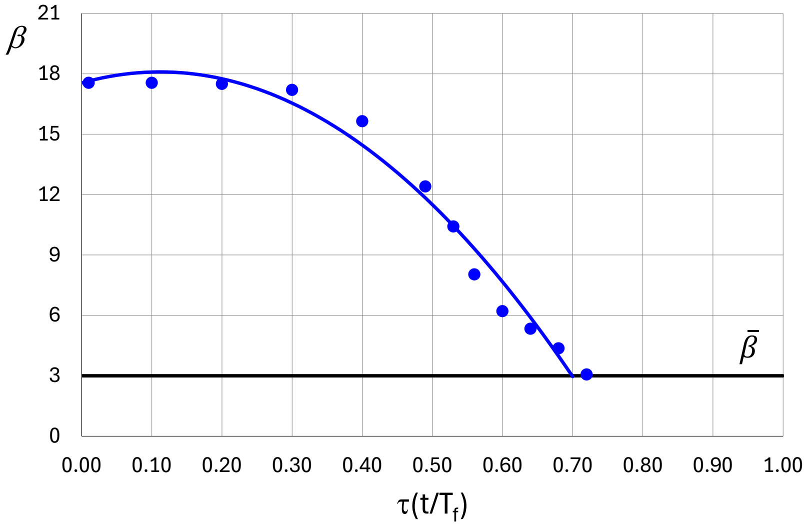

Figure 10. Experimental values of the reliability coefficient, $\beta(\tau)$ (blue dots); a polynomial function (blue curve) was used to fit the results. The horizontal line, corresponding to $\overline{\beta} = 3$, is assumed as the limit of possible failure.

Let us assume the value $\overline{\beta} = 3$ as the threshold of possible failure. Figure 10 shows that, for this value of β, the probability of attaining a failure condition occurs at a (normalized) time very close to $\tau = \frac{t}{T_f} = 0.7$, which would correspond to a survival probability of 0.9997 (see Figure 9b), i.e., to a failure probability of the order of 10^{-4}. This prediction is more restrictive than the one shown in Figure 9a, where—by observing the abscissas τ of the points of intersection between the dashed blue curves and the horizontal line identified by the threshold $SF^* = SF_{G,failure}$—the failure corresponds to a time between $0.82 \leq \tau \leq 0.90$.

4. Waiting Time Estimation for Two Different Threshold Transitions

Assuming that no further maintenance actions are undertaken with increased load that could worsen the crack pattern, it is also possible to conduct a study of the evolution of the SF_G factor over time to verify whether subsequent danger thresholds have been exceeded. This is done in order to assess the waiting time for a further worsening of the situation and to provide targeted maintenance to raise the safety level by bringing the SF_G factor back to values close to the initial ones.

For this purpose, the previously presented analysis (Figure 9) was also carried out for the threshold $SF_{G,first\ fail} = 30\%$ (Figure 11).

In Figure 11a, the evolution of the global safety factor, SF_G, over time is plotted as the performance parameter f varies. Figure 11a shows the mean value (black solid curve) and the range described by the mean + and − the standard deviation (dashed lines); the horizontal solid orange and purple lines are plotted at two different risk thresholds, $SF_{G,failure} = 20\%$ and $SF_{G,first\ fail} = 30\%$. In Figure 11b, the theoretical modelling (solid line) of the experimental reliability function (dots) is shown for the two risk thresholds analyzed. The distribution chosen for modelling it is a Gamma distribution.

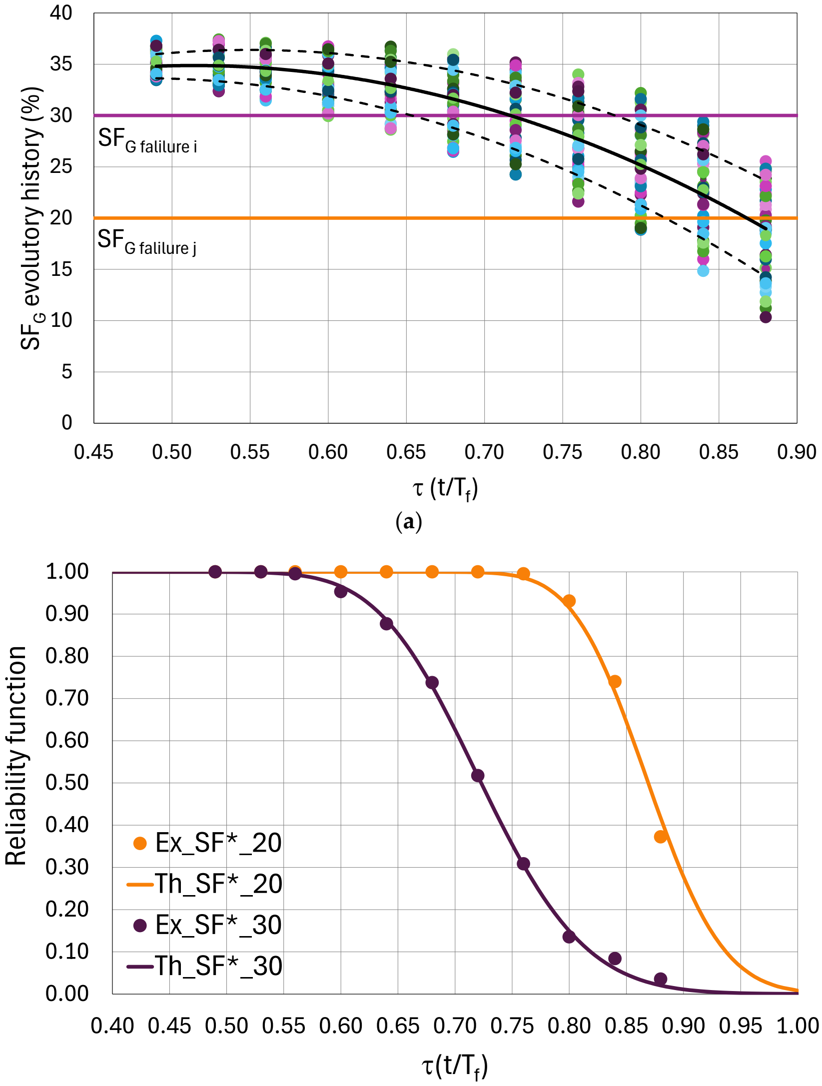

(**a**)

(**b**)

Figure 11. Evolution of the SF_G safety factors over time: (**a**) mean value (black solid curve); range described by the mean + and − the standard deviation (dashed lines); two different risk thresholds (horizontal lines); (**b**) reliability function: theoretical modelling for the two risk thresholds. $SF^* = 20\%$ (orange) and $SF^* = 30\%$ (purple) are the fixed thresholds for the global safety factor.

Based on Figure 11a, the occurrence of the $SF_{G,first\ fail}$ threshold is anticipated with respect to reaching the $SF_{G,failure}$ threshold. Note that the time interval is wider, approximately $0.65 \leq \tau \leq 0.78$, while that related to the $SF_{G,failure}$ threshold is around $0.82 \leq \tau \leq 0.90$; see also Figure 9a. In this case too, there is uncertainty in the estimation of the transition times.

Figure 11b shows the reliability curves studied for both thresholds; the early occurrence of the loss of reliability is evident when the $SF_{G,first\ fail}$ threshold is reached. The uncertainty in defining these intervals requires a probabilistic evaluation of the transition times of two different thresholds *i* and *j*, and the evaluation of any overlapping of the tails of the two distributions defining the risk area (Figure 12).

To calculate the waiting time between two threshold transitions, the following relation could be assumed:

$$\Delta T_{ij} = |T_i - T_j|, \tag{18}$$

with $T_i = \tau_i \cdot T_f$ and $T_j = \tau_j \cdot T_f$.

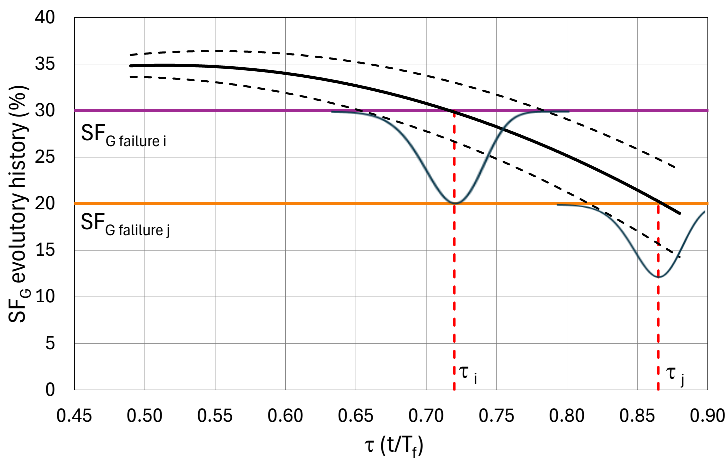

Figure 12. Qualitative uncertainty in defining the transition times of two thresholds *i* and *j*.

Given the random nature of the transition times, the values of ΔT_{ij} will have a probabilistic distribution that needs to be investigated.

The study of the reliability coefficient β once again shows a more severe alert situation (Figure 13). This situation is always close to a collapse probability of 10^{-4} for both thresholds examined (Figure 11b).

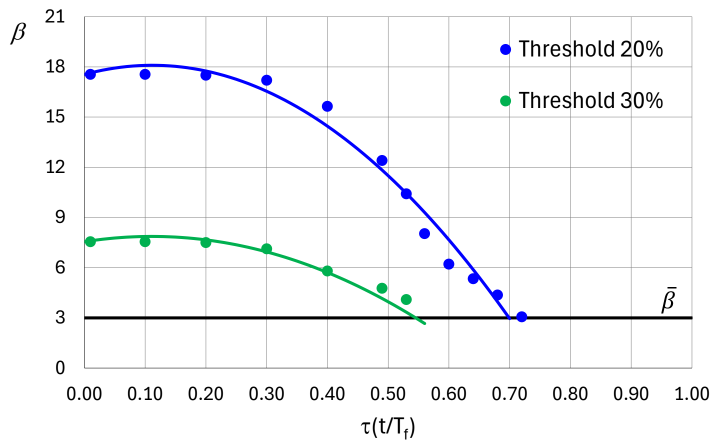

Figure 13. Time trend of the reliability coefficient, β.

5. Structural Aggravation Action on an Existing Crack Pattern

Over the course of a structure lifespan, structurally incompatible maintenance and refurbishment interventions that can worsen its structural behaviour are of multiple types and can be introduced at different times.

Therefore, a structural modification that could exacerbate the crack pattern might occur even when the performance parameter, f, related to the ongoing damage, is assumed to be less than 1. Even in this case, there are many uncertainties: What value has f reached at the time t of the damage triggered by the new action? Will the damage law change or remain the same? How much are the safety factors SF_G and SF_S and the reliability function affected?

Considering these uncertainties and variables still requires further investigation, but by assuming some simplifications—without claiming to be complete—the approach proposed here is capable of capturing the potential impact of a maintenance intervention on an existing building by assuming that it is already affected by a certain level of damage.

To this end, we study the temporal evolution of the safety factor SF_G as the performance parameter f varies, when a second intervention, with further damage initiation, is applied to an already damaged structure, with a possible increase in the existing damage. Let us now assume that the second intervention occurs at $\tau = 0.6$ and that the value of $f_2 < f_1$, with $f_1 = 1$, is a random value within the range of possible values at $\tau = 0.6$. At the instant $\tau = 0.6$, Equation (12) was used to construct a set of 100 samples of the value $\delta(\tau = 0.6)$; by applying Equation (11), we arrived at the set of values of f_2 relating to $\tau = 0.6$. Among the values obtained, the lowest value, $f_2 = 0.72$, will be used in the following, indicating greater damage and therefore a safety advantage.

The trend of the temporal evolution of the safety factor SF_G undergoes a sudden change at the moment of the triggering of the second maintenance/restoration intervention (Figure 14a), which is apparent if we compare the evolution of damage in the case with only the first intervention (see the curve ABC in Figure 14b) with the change in behaviour upon activation of the second intervention (see the curve BDE in Figure 14b). For both curves, the mean value is represented by the solid black/blue line and the range described by the mean + and − standard deviation by the dashed black/blue lines. Note that the blue curve trend in Figure 14b between points B and D is only indicative of the rapid decrease in the safety factor SF_G in the period immediately after the intervention; see the light yellow areas in Figure 14a,b. A greater accuracy in its representation would require increasing the number of instants between point B and point D. Such a decrease in this case is due to the value $f_2 = 0.72$, which is a rather severe value compared to $f_{average}(\tau = 0.6) = 0.83$ calculated as the average of the 100 values randomly extracted at $\tau = 0.6$.

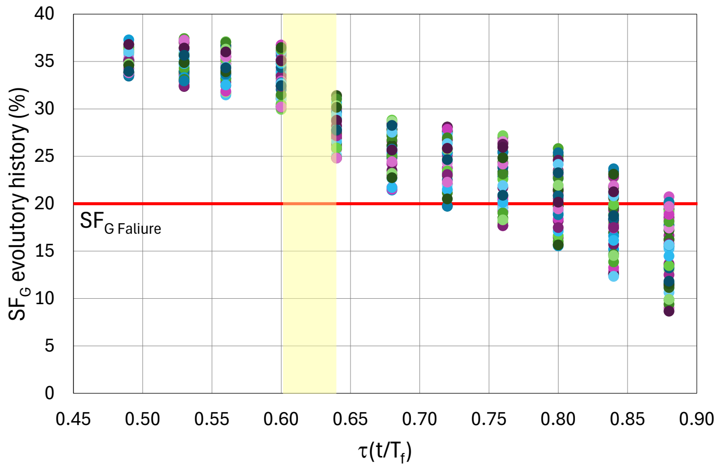

(**a**)

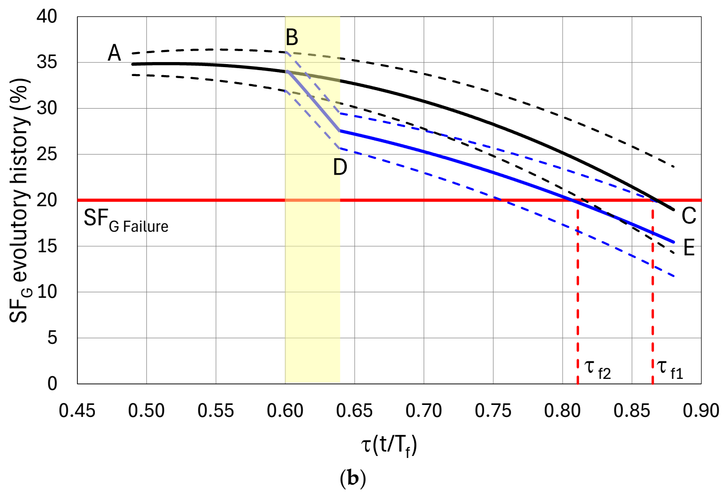

(**b**)

Figure 14. (**a**) Time evolution of the safety factor SF_G when two successive interventions are applied; (**b**) SF_G : mean values (solid lines) and range described by the mean + and − standard deviation (dashed lines): only one intervention (black curves); first and second intervention (blue curves).

From Figure 14b, however, it is clear that the failure limit will certainly be reached in a shorter time. Referring to the mean values of SF_G (black and blue solid lines), for $f_1 = 1$, we obtained $\tau_{f1} = 0.865$ and consequently $t_{f1} = 0.865\ T_f$ (see also τ_{risk} in Figure 9a), while the second damage trigger would identify $\tau_{f2} = 0.811$ corresponding to $t_{f2} = 0.811\ T_f$ (see Figure 15a), where the probability density trend of SF_G values at each instant $\tau > 0.6$ is shown. Note how the probability density curves are significantly shifted toward the failure line.

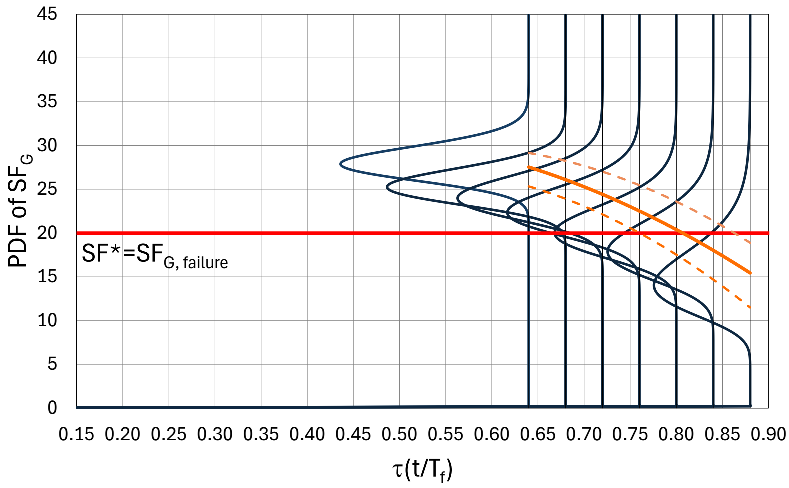

(**a**)

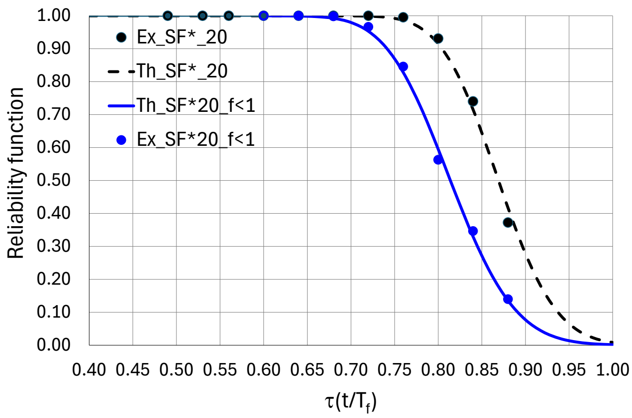

(**b**)

Figure 15. (**a**) Probability density of SF_G values for $\tau > 0.6$; (**b**) comparison of reliability curves for $f_1 = 1$ (dashed, black) and $f_2 = 0.72$ (solid, blue). $SF^* = 20\%$ is the fixed threshold for the global safety factor. The points of the experimental curve in (**b**) correspond to the areas enclosed by the PDF and above the horizontal line in (**a**).

Comparing the reliability curves shown in Figure 15b, for the initiation of the second damage event, the reliability curve describes a probability of performance reduction in the order of 10^{-4} already for values of τ close to 0.6, while for the initiation of the first damage event, these values are recorded for τ approximately equal to 0.7.

For clarity, it should be noted that the results presented here for illustrative purposes refer to a true change in intended use, from residential to commercial, often implemented in the historic centres of Lombardy cities. The opening of windows in the ground floor perimeter walls resulted in a reduction in the area of their horizontal cross-sections, without restoring the shear capacity provided by the original masonry.

6. Safety Factor and Failure Time in Case of Subsequent Damage Triggers

As can be seen from the previous section, each further damage triggering compromises the safety factor and the resulting failure time (Figure 14b).

By generalizing the problem (Figure 16), it can be stated that the critical time for exceeding the threshold $SF^* = SF_{G,failure}$ can be given by the minimum of the times related to the triggering of a subsequent damage event.

$$T_{critical} = \min\left\{ t \middle| SF_{G,k}(t) \le SF_{G,failure} \right\}, \quad (19)$$

with $t = \tau \cdot T_f$, while the waiting time between two possible failures is given by Equation (18). This value provides information on the time available to operators to intervene with structural improvement actions before the system reaches the failure limit.

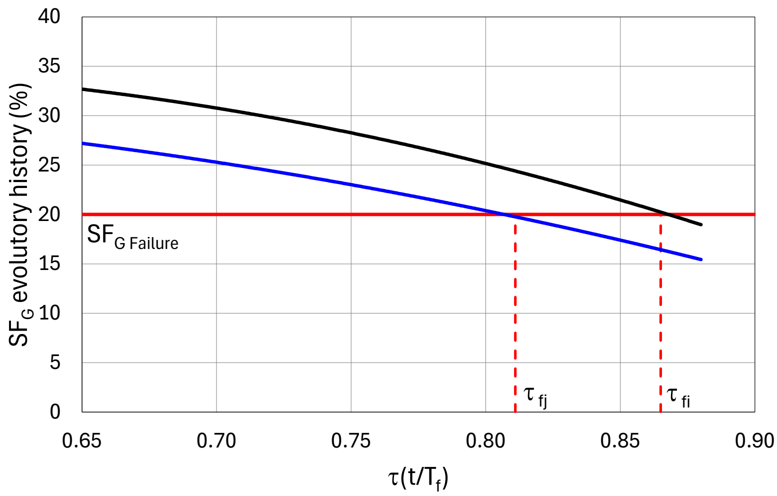

Figure 16. Evolution history of the safety factor SF_G after two successive interventions (black and blue curves) with relative damage triggering (blue curve: SF_G reduction).

In the presented case, considering the results of the accelerated experimental analyses mentioned in Section 2.2 [21,22], the failure time $T_f^{(a)} = 890$ days could be assimilated to a real failure time T_f of about 400 years [31,32,41–44]; the waiting interval between the first damage trigger and the second damage trigger is then

$$\Delta T_{12} = 0.865 \cdot 400 - 0.811 \cdot 400 = 21.6 \text{ years} \quad (20)$$

From Equation (18), the failure condition due to the first and second maintenance interventions with damage triggering could be attained at $T_{critic} = 324.4$ years. If we assume a nominal lifetime of 100 years, as imposed by the Italian Standard, NTC2018 [25], we obtain: $\Delta T_{12} = 5.4$ years and $T_{critic} = 81.1$ years. It is also true that interventions that are structurally incompatible and can cause damage are usually modern, dating back only to the last 100 years (i.e., the 20th century).

7. Discussion: The Problem of Uncertainties

The case study described above provides an example in which only some uncertainties have already been taken into account. It should be observed that:

(1) The evolution of the safety factor SF_G is uncertain from the start of construction of the building. The uncertainties are mainly due to the mechanical characteristics of the materials, which, according to regulations [17], can follow a probabilistic distribution [15,20].

(2) The triggering of the first (potentially damaging) refurbishment intervention can occur at a time when the safety factor SF_G is no longer at its maximum level while maintaining the performance factor $f = 1$, i.e., excluding any ongoing cracking pattern.
(3) The triggering of the second (potentially damaging) intervention can occur for $f < 1$ with uncertain values (Equation (11)); uncertainty affects also the global safety factor, SF_G, whose value will follow a probability distribution (Figure 9a).
(4) The evolution of the safety factor after the triggering of the second damaging intervention is uncertain (Figure 15a).
(5) As a consequence of the uncertainties mentioned above, the transition times, τ_{fi} and τ_{fj}, of the $SF^* = SF_{G,failure}$ threshold for two successive damaging situations will have a probabilistic distribution (Figure 17).

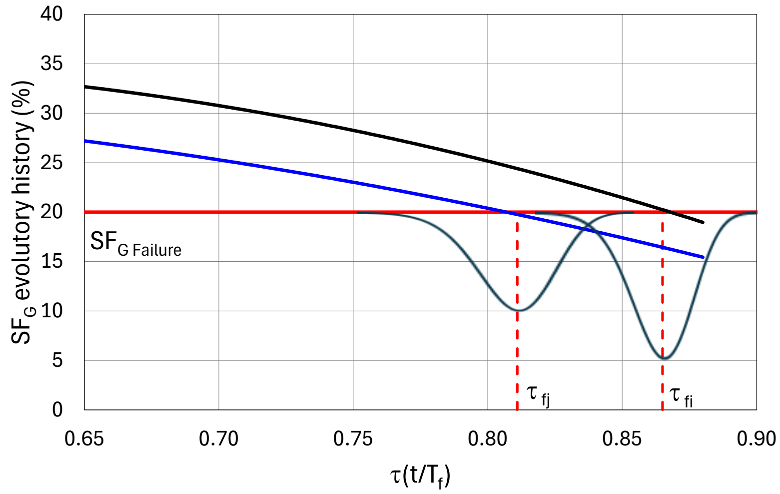

Figure 17. Evolution history of the safety factor SF_G after two successive interventions (black and blue curves). Qualitative modelling of the possible uncertainties in the definition of the normalized times, τ_{fi} and τ_{fj}, corresponding to the achievement of the SF_G threshold ($SF_G = SF^* = SF_{G,failure}$).

(6) Therefore, the waiting time between two possible failures due to two subsequent damage triggers will also be a probability distribution (Figure 18).

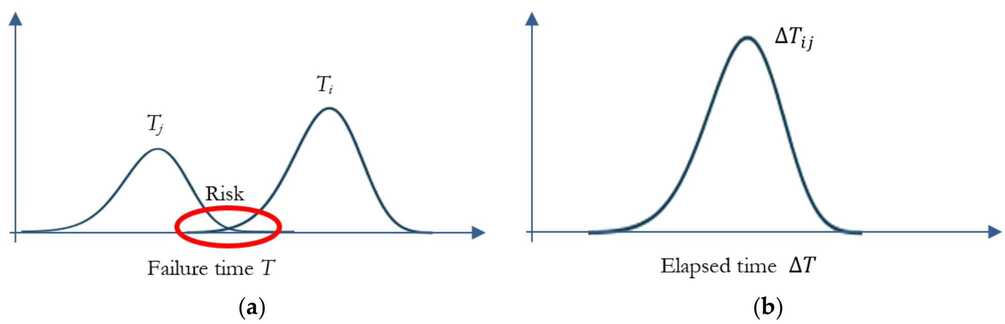

Figure 18. (**a**) Qualitative distribution of failure times due to two successive damage triggers; (**b**) qualitative distribution of waiting times between two possible failures due to two successive damage triggers.

8. Conclusions

This work tackles the issue of the variation in the static safety factor and the global safety factor when damage is caused by extraordinary maintenance and refurbishment interventions on existing masonry structures that are structurally incompatible and likely to cause greater stress to the original structures. The research aims to also consider the aspect of long-term consequences on the damage progression in the masonry.

It can be noted how both the static and the global safety factors decrease while all other parameters (geometric and seismic) remain unchanged, even examining the situation created by only the first intervention (from the start of construction), considering the uncertainties that could arise from the damage evolution (probabilistic approach).

This investigation helps assess the reliability of the building system over time. Furthermore, it can provide information on the waiting time required to overcome two different failure thresholds.

Another aspect of the uncertainty examined was the assessment of the change in system reliability if further modifications were made to the building in the presence of an already active crack pattern, without removing the damaging cause, i.e., assuming $f < 1$, at the time of the new intervention. There are multiple uncertainties that emerge from this analysis: (a) the value to be associated with the performance parameter f; (b) the value of the global safety factor SF_G achieved in the system after the second intervention; and (c) its trend over time.

The results obtained for a case study, represented by ordinary residential masonry buildings presented in nearly all historic centres of Milan hinterland, showed how important it is to take such uncertainties into account and how it is inevitable to approach the study of such problems from a probabilistic point of view.

To address these uncertainties, this research proposed the study of a degradation law for the performance parameter f, based on long-term laboratory analyses suitable for simulating cracking behaviour due only to the increase in permanent and long-term loads, a Monte Carlo simulation approach for the creation of a sample of possible values of the SF_G safety factor over time as the f parameter varies, and subsequent probabilistic modelling both for the SF_G values at each analyzed instant and for the construction of the theoretical reliability curve.

The results showed how a careless maintenance intervention, on a system already affected by an ongoing cracking pattern, anticipates the reaching of a risk threshold. The waiting interval ΔT_{ij} between two failures is also uncertain and should be verified with appropriate probabilistic analyses.

A further development of the current study will be to investigate the temporal variation in the global safety factor SF_G as local seismicity varies. The global safety factor could also help determine whether a structure with good characteristics for a given seismic zone, characterized by a certain spectrum, could also be suitable for more "severe" seismic zones or different types of topography/subsoil.

Further application aspects related to the procedure proposed here concern the conservation of the architectural heritage. Indeed, it is worth noting that, in the context of the preservation of masonry structures, design criteria and construction techniques must be chosen in such a way as to avoid reducing both local and global safety factors. The greatest risk in restoration interventions or in the maintenance of masonry buildings is underestimating the consequences of careless demolition, which can compromise the stability of the building, or the traumatic insertion of new structural elements into the existing masonry (e.g., replacing floors). For this reason, the procedure proposed here can represent a significant tool to capture the effects of incorrect maintenance strategies, since it takes into account both the load variation and the damage due to such interventions, associated with the decrease in masonry strength, through the performance parameter f. As already mentioned, the results relating to the case study in question correspond to an actual change in intended use: from residential to commercial. The next phases of the research will focus on demonstrating the method's reliability even in the presence of further modifications, such as additions to stories and other types of changes in use, which subject the structure to greater loads.

In this regard, it is worth emphasizing that the proposed method requires knowledge of only a few parameters, namely the building geometry and the mechanical characteristics of the masonry, making it potentially applicable to buildings and masonry types other than the case study considered here for illustrative purposes. Its main limitation is undoubtedly that, being a rapid method, it is unable to capture the local stresses and critical issues that more sophisticated approaches can highlight. However, rapid analysis can be extended to all historic buildings in a city with reduced execution times and costs, providing managers with a hierarchy of problems and relative urgency for further investigation and possible interventions.

Author Contributions: Conceptualization, E.G., G.C. and D.A.; methodology, E.G., G.C. and D.A.; software, E.G.; validation, E.G., G.C. and D.A.; formal analysis, E.G., G.C. and D.A.; data curation, E.G.; investigation, E.G., G.C. and D.A.; writing—original draft preparation, E.G. and D.A.; writing—review and editing, E.G., G.C. and D.A.; visualization, G.C.; supervision, E.G.; project administration, E.G. and G.C.; funding acquisition, E.G. and G.C. All authors have read and agreed to the published version of the manuscript.

Funding: This research was funded by The DPC-ReLUIS 2024–2026 Project, work packages WP13—*Ciclo di vita e sostenibilità di costruzioni e infrastrutture*—and WP4—*Mappe di rischio e scenari di danno sismico MARS-CARTIS*, CUP D57G24000100001.

Data Availability Statement: The data that support the findings of this study are available on request from the corresponding author, D.A.

Conflicts of Interest: The authors declare no conflicts of interest.

Appendix A

Appendix A.1

The behaviour factor, q (see relation (2)), can be assumed to be 3 for buildings with regular elevation, and 2.25 in other cases.

Appendix A.2

Since masonry buildings primarily behave like boxes, the vibration modes are similar to those of a cantilever with all the mass participating in the motion. When the participation factor e^* is set to 1 (for safety reasons), it indicates that the mass participates 100%.

Appendix A.3

According to [3,17], the formal expression of the design value of the shear strength in the masonry walls of floor i, τ_{di}, is $\tau_{di} = \tau_{0,d}\sqrt{1+\frac{\sigma_{0,i}}{1.5\tau_{0,d}}}$, where $\tau_{0,d}$ is the value of the masonry shear strength; in the case of different types of walls on the same floor, the average value of $\tau_{0,d}$ should be used.

Appendix A.4

According to the Italian standard, S $= S_S S_T$ (see Equation (1)), where S_S is the stratigraphic amplification coefficient (see [25], Table 3.2.V) and S_T is the topographic amplification coefficient (see [25], Table 3.2.VI). In the current application, $S_T = 1$, $S_S = 1.39$ (topography T1, subsoil type C = medium-densified coarse-grained and very consistent fine-grained).

F_0, the spectral amplification factor at the *Stato Limite di salvaguardia della Vita* (SLV) (Life-saving Limit State for the site) (see Equation (2)), depends on the seismic zone where the building is located. For Italy, its value can be found on the *Istituto Nazionale di Geofisica e Vulcanologia* (INGV) website or in the Excel spreadsheets of the *Department of Civil Protection* for calculating seismic response spectra. It corresponds to the maximum value of the normalized spectrum $C(T)$—obtained as the ratio between the elastic response spectrum (see [25], point 3.2.3.2.1) and the spectral acceleration that takes into account the site characteristics (a_gS)—i.e., to the plateau of the constant acceleration portion of the spectrum. As observed by [3], this simplification can have a significant impact on low-rise (single-story) masonry buildings on type C or D soils, for which the oscillation period is shorter than that corresponding to the initial portion of the spectrum plateau. To account for these simplifying assumptions, the coefficient r was introduced by [1–3]; see Equation (2).

References

1. Borri, A.; De Maria, A.; Casaglia, S. The EAL-M method for the seismic classification of the existing masonry buildings: A comparison between different methods and preliminary evaluations of other typologies. *Progett. Sismica* **2014**, *5*, 11–29. (In Italian)
2. Borri, A.; Corradi, M.; Castori, G.; De Maria, A. A method for the analysis and classification of historic masonry. *Bull. Earthq. Eng.* **2015**, *13*, 2647–2665. [CrossRef]
3. Borri, A.; De Maria, A. La Classificazione Sismica: Un Protocollo Metodologico Già Operativo Applicabile Agli Edifici Esistenti in murature. *Ingegno-web*. 2016. Available online: https://www.ingenio-web.it (accessed on 1 December 2025).
4. Preciado, A.; Ramirez-Gaytan, A.; Santos, J.C.; Rodriguez, O. Seismic vulnerability assessment and reduction at a territorial scale on masonry and adobe housing by rapid vulnerability indicators: The case of Tlajomulco, Mexico. *Int. J. Disaster Risk Reduct.* **2020**, *44*, 101425. [CrossRef]
5. Mascheri, G.; Chieffo, N.; Lourenço, P.B. Multi-attribute-based procedure for seismic loss scenario in a historical area. *Bull. Earthq. Eng.* **2024**, *22*, 7323–7358. [CrossRef]
6. Silva, V.; Crowley, H.; Varum, H.; Pinho, R. Seismic risk assessment for mainland Portugal. *Bull. Earthq. Eng.* **2015**, *13*, 429–457. [CrossRef]
7. Silva, V. Critical issues in probabilistic earthquake loss assessment. *J. Earthq. Eng.* **2018**, *22*, 1683–1709. [CrossRef]
8. Dolce, M.; Prota, A.; Borzi, B.; da Porto, F.; Lagomarsino, S.; Magenes, G.; Moroni, C.; Penna, A.; Polese, M.; Speranza, E.; et al. Seismic risk assessment of residential buildings in Italy. *Bull. Earthq. Eng.* **2021**, *19*, 2999–3032. [CrossRef]
9. Vona, M.; Flora, A.; Carlucci, E.; Foscolo, E. Seismic Retrofitting Resilience-Based for Strategic RC Buildings. *Buildings* **2021**, *11*, 111. [CrossRef]
10. Mina, D.; Forcellini, D.; Karampour, H. Analytical fragility curves for assessment of the seismic vulnerability of HP/HT unburied subsea pipelines. *Soil Dyn. Earthq. Eng.* **2020**, *137*, 106308. [CrossRef]
11. Flora, A.; Perrone, G.; Cardone, D. Evaluating Collapse Fragility Curves for Existing Buildings Retrofitted Using Seismic Isolation. *Appl. Sci.* **2020**, *10*, 2844. [CrossRef]
12. Akhoondi, M.R.; Behnamfar, F. Seismic fragility curves of steel structures including soil-structure interaction and variation of soil parameters. *Soil Dyn. Earthq. Eng.* **2021**, *143*, 106609. [CrossRef]
13. Gallardo, J.A.; de la Llera, J.C. Epistemic uncertainty in the seismic performance assessment of isolated buildings due to high damping rubber bearing model selection. *Eng. Struct.* **2026**, *348*, 121734. [CrossRef]
14. Cardani, G.; Garavaglia, E. Seismic Vulnerability Assessment of Historic Centers with Two Fast Methods Based on CARTIS Survey Methodology and Fragility Curves. *Heritage* **2024**, *7*, 5356–5372. [CrossRef]
15. Cardani, G.; Garavaglia, E.; Aita, D. A Rapid Seismic Classification of Historic Masonry Buildings with Risk Matrices. In Proceedings of the 43rd National Conference, GNGTS, Bologna, Italy, 11–14 February 2025. Session 2.2. Book of Abstract, Extended Abstract. 1–7. GNGTS 2025 Abstracts—Google Drive.
16. Angjeliu, G.; Cardani, G.; Garavaglia, E. Rapid assessment of seismic vulnerability of historic masonry structures through fragility curves approach and national database data. *Dev. Built Environ.* **2023**, *14*, 100140. [CrossRef]
17. *CNR-DT 212/2013*; Istruzioni per la Valutazione Affidabilistica della Sicurezza Sismica di Edifici Esistenti. Commissione di Studio per la Predisposizione e L'analisi di Norme Tecniche Relative Alle Costruzioni: Rome, Italy, 2014.
18. Cons. Sup. LL. PP., Circular No. 617 of February 02, 2009. Istruzioni per L'applicazione delle 'Nuove Norme Tecniche per le Costruzioni' di cui al Decreto Ministeriale del 14.01.2008. (Published in Gazzetta Ufficiale, Serie Generale, No. 47 of 26/02/2009, Suppl. Ord. No. 27). Available online: https://www.gazzettaufficiale.it/eli/id/2009/02/26/09A01318/sg (accessed on 1 December 2025).

19. Cons. Sup. LL. PP., Circular No. 7 of January 21, 2019. Istruzioni per L'applicazione dell'«Aggiornamento delle "Norme Tecniche per le Costruzioni"» di cui al Decreto Ministeriale 17 Gennaio 2018. (Published in Gazzetta Ufficiale, Serie Generale, No. 35 of 11/02/2019, Suppl. Ord. No. 5). Available online: https://www.gazzettaufficiale.it/eli/id/2019/02/11/19A00855/sg (accessed on 1 December 2025).
20. Garavaglia, E.; Cardani, G.; Aita, D. On the Safety of Damaged Masonry Structures: A First Probabilistic Approach. In *Proceedings of the 4th International Conference of Steel and Composite for Engineering Structures, ICSCES 2025, Piacenza, Italy, 9–12 July 2025*; Lecture Notes in Civil Engineering; Milani, G., Magagnini, E., Khatir, S., Eds.; Springer: Cham, Switzerland, 2025; Volume 746, pp. 725–733.
21. Anzani, A.; Garavaglia, E.; Binda, L. Long-term damage of historic masonry: A probabilistic model. *Constr. Build. Mater.* **2009**, *23*, 713–724. [CrossRef]
22. Garavaglia, E.; Cardani, G.; Anzani, A. Probabilistic Modelling of Aging Masonry. In *Long-Term Performance and Durability of Masonry Structures*; Ghiassi, B., Lourenço, P.B., Eds.; Woodhead Publishing Series in Civil and Structural Engineering: Cambridge, UK, 2019; pp. 367–390.
23. Turnsek, V.; Cacovic, F. Some Experimental Results on the Strength of Brick Masonry Walls. In *Proceedings of the 2nd International Brick Masonry Conference, Stoke-on-Trent, UK, 12–15 April 1970*; British Ceramic Research Association: Stoke-on-Trent, UK, 1971; pp. 149–156.
24. Decreto del Ministero delle Infrastrutture 14 gennaio 2008 [Decree of the Ministry of Infrastructure dated January 14, 2008], Approvazione delle nuove norme tecniche per le costruzioni. (Published in Gazzetta Ufficiale No. 29 of 04/02/2008, Suppl. Ord. No. 30). Available online: https://www.gazzettaufficiale.it/atto/vediMenuHTML?atto.dataPubblicazioneGazzetta=2008-02-04&atto.codiceRedazionale=08A00368&tipoSerie=serie_generale&tipoVigenza=originario (accessed on 1 December 2025).
25. Decreto del Ministero delle Infrastrutture 17 gennaio 2018 [Decree of the Ministry of Infrastructure dated January 17, 2018], NTC2018 Aggiornamento delle «Norme tecniche per le costruzioni». (Published in Gazzetta Ufficiale No. 42 of 20/02/2018, Suppl. Ord. No. 8). Available online: https://www.gazzettaufficiale.it/atto/vediMenuHTML?atto.dataPubblicazioneGazzetta=2018-02-20&atto.codiceRedazionale=18A00716&tipoSerie=serie_generale&tipoVigenza=originario (accessed on 1 December 2025).
26. Foraboschi, P.; Vanin, A. Experimental investigation on bricks from historical Venetian buildings subjected to moisture and salt crystallization. *Eng. Fail. Anal.* **2014**, *45*, 185–203. [CrossRef]
27. Saviano, F.; Lignola, G.P.; Parisi, F. Experimental compressive and shear behaviour of clay brick masonry with degraded joints. *Constr. Build. Mater.* **2024**, *452*, 138880. [CrossRef]
28. Biondini, F.; Frangopol, D.M.; Garavaglia, E. Life-Cycle Reliability Analysis and Selective Maintenance of Deteriorating Structures. In *Proceedings of the International Symposium on Life-Cycle Civil Engineering, IALCCE '08, Varenna, Como, Italy, 11–14 June 2008*; Biondini, F., Frangopol, D.M., Eds.; Taylor & Francis Groups: London, UK, 2008; pp. 483–488.
29. Garavaglia, E.; Basso, N.; Sgambi, L. The Markovian Approach for Probabilistic Life-Cycle Assessment of Existing Structures. *Appl. Math.* **2012**, *3*, 2080–2088. [CrossRef]
30. Garavaglia, E.; Basso, N.; Sgambi, L. Probabilistic life-cycle assessment and rehabilitation strategies for deteriorating structures: A case study. *Int. J. Arch. Herit.* **2018**, *12*, 981–996. [CrossRef]
31. Garavaglia, E.; Gianni, A.; Molina, C. Reliability of porous materials: Two stochastic approaches. *J. Mater. Civ. Eng.* **2004**, *16*, 419–426. [CrossRef]
32. Binda, L.; Molina, C. Building Materials Durability Semi-Markov Approach. *J. Mater. Civ. Eng.* **1990**, *2*, 223–239. [CrossRef]
33. Pisano, B. Le Rigidezze Fessurate in Condizioni Sismiche. Pisano Ingegneria 2017. Available online: https://www.pisanoingegneria.it/2017/07/31/le-rigidezze-fessurate-in-condizioni-sismiche/ (accessed on 24 November 2025).
34. Dauda, J.A.; Iuorio, O.; Muhit, I.B.; da Silva, L.C.M. Systematic review of experimental testing of masonry walls' failure: Comparative analysis and future directions. *Eng. Fail. Anal.* **2024**, *163*, 108571. [CrossRef]
35. Ordinanza del Presidente del Consiglio dei Ministri [Ordinance of President of the Council of Ministers] No. 3519 of 28 April 2006, Criteri generali per L'individuazione delle zone Sismiche e per la formazione e l'aggiornamento degli Elenchi delle medesime zone. (Published in Gazzetta Ufficiale, Serie Generale No. 108 of 11/05/2006). Available online: https://www.gazzettaufficiale.it/eli/id/2006/05/11/06A04427/sg (accessed on 1 December 2025).
36. Evans, D.H. *Probability and Its Applications for Engineers*; Marcel Dekker Inc.: New York, NY, USA, 1992.
37. Wenocur, M.L. A reliability model based on the gamma process and its analytic theory. *Adv. Appl. Probab.* **1989**, *21*, 899–918. [CrossRef]
38. Iervolino, I.; Chioccarelli, E.; Giorgio, M. Gamma modeling of continuous deterioration and cumulative damage in life-cycle analysis of earthquake-resistant structures. In *Proceedings of the ICOSSAR 2013, 11th International Conference on Structural Safety, Reliability, Risk and Life-Cycle Performance of Structures & Infrastructures, New York, NY, USA, 16–20 June 2013*; Deodatis, G., Ellingwood, B.R., Dan, M., Frangopol, D.M., Eds.; Taylor & Francis Group: London, UK, 2013; pp. 1–8, ISBN 978-1–138-00086-5.
39. van Noortwijk, J.M.; van der Weide, J.A.M.; Kallen, M.J.; Pandey, M.D. Gamma processes and peaks-over-threshold distributions for time-dependent reliability. *Reliab. Eng. Syst. Saf.* **2007**, *92*, 1651–1658. [CrossRef]

40. Biondini, F.; Frangopol, D.M. Life-Cycle Performance of Deteriorating Structural Systems under Uncertainty: Review. *J. Struct. Eng.* **2016**, *142*, F4016001. [CrossRef]
41. Binda, L. (Ed.) *Learning from Failure Long-Term Behaviour of Heavy Masonry Structures*; WIT Press: Southampton, UK, 2007; ISBN 978-1-84564-057-6.
42. Binda, L.; Gatti, G.; Mangano, G.; Poggi, C.; Sacchi Landriani, G. La Torre Civica di Pavia: Indagini sui materiali e sulla struttura. *L'Edilizia E L'Industrializzazione* **1990**, *11*, 713–735.
43. Binda, L.; Anzani, A.; Saisi, A. Failure Due to Long Term Behaviour of Heavy Structures: The Pavia Civic Tower and the Noto Cathedral. In *Proceedings of the 8th International Conference on STREMAH 2003, Structures Studies Repairs and Maintenance of Heritage Architecture, Halkidiki, Greece, 7–9 May 2003*; WIT Press: Southampton, UK, 2003; pp. 99–108.
44. Binda, L.; Anzani, A.; Saisi, A. Danneggiamento progressivo di edifici storici in muratura. Ricerche dopo il crollo della Torre Civica di Pavia. In *Proceedings of the Convegno Nazionale Sperimentazione su Materiali e Strutture, Venezia, Italy, 6–7 December 2006*; Russo, S., Siviero, E., Vita, G., Eds.; Pavia University Press: Pavia, Italy, 2006; pp. 17–22.